Single-particle and collective structures in ^{55}Cr and ^{55}V

A. N. Deacon,[1,*] D. Steppenbeck,[1,†] S. Zhu,[2] S. J. Freeman,[1] R. V. F. Janssens,[2] M. P. Carpenter,[2] B. Fornal,[3] M. Honma,[4]
B. P. Kay,[1,‡] F. G. Kondev,[2] J. Kozemczak,[5] A. Larabee,[5] T. Lauritsen,[2] C. J. Lister,[2] A. P. Robinson,[2,§] D. Seweryniak,[2]
J. F. Smith,[1,∥] Y. Sun,[6,7,8] X. Wang,[2,¶] F. R. Xu,[9] and Y.-C. Yang[6]

[1]*Schuster Laboratory, University of Manchester, Manchester M13 9PL, United Kingdom*
[2]*Argonne National Laboratory, Argonne, Illinois 60439, USA*
[3]*Institute of Nuclear Physics, Polish Academy of Sciences, PL-31342 Krakow, Poland*
[4]*Center for Mathematical Sciences, University of Aizu, Tsuruga, Ikki-machi, Aizu-Wakamatsu, Fukushima 965-8580, Japan*
[5]*Physics Department, Greenville College, Greenville, Illinois 62246, USA*
[6]*Department of Physics, Shanghai Jiao Tong University, Shanghai 200240, People's Republic of China*
[7]*Institute of Modern Physics, Chinese Academy of Sciences, Lanzhou 730000, People's Republic of China*
[8]*Department of Physics and Astronomy, University of Tennessee, Knoxville, Tennessee 37996, USA*
[9]*Department of Technical Physics, Peking University, Beijing 100871, People's Republic of China*

Excited states in ^{55}V and ^{55}Cr have been populated via pn and $2n$ evaporation channels, respectively, following the fusion of a ^{48}Ca beam at 172 MeV with a ^{9}Be target. Level schemes have been deduced for the two nuclides to excitation energies of 7467 (^{55}V) and 12226 keV (^{55}Cr), with spins of $27/2^+$ and $33/2^+$, respectively. Negative-parity states are compared with shell-model calculations using three different effective interactions in the full fp model space. Negative-parity levels of ^{55}Cr are explained in terms of single-particle fp-shell configurations outside $N = 28$ and $N = 32$ cores. Positive-parity states in both isotopes show evidence for the involvement of neutron $g_{9/2}$ configurations. In the case of ^{55}Cr, a quasirotational structure based on the $1/2^+[440]$ Nilsson orbital is observed up to the terminating state. In ^{55}V, positive-parity states do not exhibit well-developed collective features, and the observation of octupole decays is an indication of their importance in transitions from neutron $g_{9/2}$ configurations to the fp shell. Experimental results are compared with the predictions of a traditional shell model, the projected shell model, and total-Routhian-surface calculations.

I. INTRODUCTION

The evolution of nuclear shell structure is a topic under much current scrutiny because magic numbers that are well established in near-stable nuclei have been found to alter away from the line of stability. The neutron-rich fp-shell nuclei, bounded by $20 \leqslant Z \leqslant 28$ and $28 \leqslant N \leqslant 40$, represent one region of the nuclear chart where significant developments have occurred recently. For example, experimental evidence points to the opening of a new shell gap at $N = 32$ in neutron-rich nuclei close to Ca; systematics of $E(2_1^+)$ values beyond $N = 28$ [1–7] show a sharp rise at $N = 32$ associated with a relatively large $p_{3/2} - p_{1/2}$ separation. This effect weakens for nuclei with increasing Z as movements of the neutron $f_{5/2}$ orbital, due to increasing interactions with $f_{7/2}$ protons,

effectively destroy the gap between orbitals. The presence of this subshell closure has been confirmed in investigations of transition probabilities where low $B(E2; 0_{\mathrm{g.s.}}^+ \to 2_1^+)$ rates have been measured in ^{54}Ti [7] and ^{56}Cr [8].

The theoretical understanding of shell evolution has progressed in a number of ways and includes the development of new effective interactions for shell-model calculations within large extended model spaces. For example, the introduction of the GXPF1 interaction [9] enabled an understanding of the evolving nature of the $N = 32$ gap in the neutron-rich fp shell, providing a good description of both first excited states near the subshell closure and some observed high-spin states [4,10]. GXPF1 calculations also predict an additional shell gap to arise at $N = 34$; experimental evidence for this effect, however, remains elusive. The lack of an observed gap between the $\nu p_{1/2}$ and $\nu f_{5/2}$ orbitals [5,6,11] and measurements of the $B(E2; 0_{\mathrm{g.s.}}^+ \to 2_1^+)$ transition rate in ^{56}Ti [7] suggest that a substantial subshell closure does not persist above $Z = 20$. It appears that the changes in the effective single-particle energy of the $\nu f_{5/2}$ orbital are not predicted quite correctly in GXPF1 calculations. These observations prompted modifications resulting in a more refined interaction, GXPF1A [12], where the effective single-particle energies of the $\nu f_{5/2}$ and $\nu p_{3/2}$ states are closer and in which five $T = 1$ matrix elements of the interaction are adjusted. This led to significant improvements in the predictive power of the calculations; the value of $E(2_1^+)$ in ^{56}Ti, for example, is reduced

───────────
*alick.deacon@manchester.ac.uk

†Present address: RIKEN Nishina Center, 2-1, Hirosawa, Wako, Saitama 351-0198, Japan.

‡Present address: Department of Physics, University of York, Heslington, York YO10 5DD, United Kingdom.

§Present address: Schuster Laboratory, University of Manchester, Manchester M13 9PL, United Kingdom.

∥Present address: School of Engineering, University of the West of Scotland, High Street, Paisley PA1 2BE, United Kingdom.

¶Present address: Department of Physics, Florida State University, Tallahassee, Florida 32306, USA.

to give much better agreement with experiment than was the case with the GXPF1 interaction, and a consistent description of the structure of all the neutron-rich Ti isotopes [5,10,11,13] is achieved. More recently, further modifications to the GXPF1 family of interactions [14] have produced closer fits to experimental data on $^{51-53}$Ca [15]. This GXPF1B interaction resulted from an increase in the $p_{1/2}$ single-particle energy by 0.3 MeV and further readjustments to the pairing matrix elements relating to the $p_{1/2}$ orbital and the $T = 1$ diagonal two-body matrix element for the $p_{3/2} - p_{1/2}$ states, making the quadrupole-quadrupole interaction stronger. However, this interaction is still regarded as somewhat tentative and thus requires further testing by comparison with new experimental data.

As noted above, experimental studies in the neutron-rich fp shell have stimulated the development of shell-model interactions for neutron excitations with rather successful outcomes, even if the particular question of a possible $N = 34$ gap in calcium isotopes remains unanswered (see Refs. [16] and [17] for more details). It is difficult to make the same claim for the understanding of proton configurations. The population of cross-shell excitations in ^{52}Ca by two-proton knockout reactions have highlighted the less satisfactory description of proton excitations using the existing interactions [18], and it is clear that there is room for significant improvement.

Deeper into the middle of the fp shell, evidence is accumulating for the development of collectivity thought to be associated with excitations of neutrons across the $N = 40$ shell gap populating configurations involving the deformation-driving $\nu g_{9/2}$ orbital, particularly in chromium and iron isotopes. The low-lying states of the even chromium isotopes exhibit first-excited-state energies that are consistent with developing collectivity toward $N = 40$. Indeed, the development of large deformation in the low-lying states of ^{62}Cr is also evident in measurements of cross sections from proton inelastic scattering [19]. The recent extension of the knowledge of excited states to ^{64}Cr [20] displays a continued fall in the $E(2_1^+)$ values and a corresponding rise in the ratio $E(4_1^+)/E(2_1^+)$ at $N = 40$, indicating the collective nature of these levels. Higher-spin states in less exotic systems also point to the importance of the $\nu g_{9/2}$ orbital with negative-parity side structures observed in ^{56,58}Cr [21]. There is also a notable compression of the yrast band in ^{60}Cr relative to fp shell-model calculations, which is indicative of the presence of configurations outside this model space [21]. Additionally, the odd-A neutron-rich Cr isotopes display signs of collectivity. The ^{57}Cr nucleus has a quasirotational band of positive-parity states observed to high spin [22] that has been interpreted as being associated with moderate prolate deformation, arising from a $1/2^+[440]$ configuration of spherical $g_{9/2}$ parentage. In ^{59}Cr, however, the situation is less certain. A low-lying isomeric $9/2^+$ level has been interpreted as the band head of a $9/2^+[404]$ configuration, leading to the polarization of a mildly oblate core toward a well-deformed oblate shape [22,23]. However, a similar long-lived $9/2^+$ state in ^{61}Fe has been associated with prolate deformation and a rotation-aligned coupling scheme [24].

In the other iron isotopes, the 2_1^+ systematics concur with the picture of increasing collectivity but suggest some differences

in its development compared to chromium isotopes [20]. The extent of the collectivity has been quantified recently with lifetime measurements in ^{62,64,66}Fe [25]. The enlargement of the fp space to include the $\nu g_{9/2}$ orbital presents significant theoretical challenges, although steps forward are being made with the development of the appropriate fpg interactions, both in traditional approaches and in projected shell-model methods [20,25–29].

This paper presents results on two of the $A = 55$ isobars in the neutron-rich fp-shell region, $^{55}_{23}$V and $^{55}_{24}$Cr, with the dual aims of testing further the effective interactions and approaches used in shell-model calculations and of exploring the signatures associated with collectivity in these isotopes. Initial results on ^{55}V have previously been presented by Zhu *et al.* [13]. The current work provides some revisions to the spin and parity assignments proposed previously, enabling the interpretation of the structure of ^{55}V to be revisited. The data are compared with the results of shell-model calculations using a number of interactions to test the recently proposed modifications and assessing the role of protons in this isotope. It should be noted that a detailed analysis of the level structure of ^{52}Ti, including lifetime measurements based on line shapes from data obtained in the same experiment, has already provided extensive tests of effective interactions in that isotope [30]. In addition to a comparison of the low-lying states with fp models, the results on ^{55}Cr presented here show further evidence of the involvement of the $g_{9/2}$ orbital in higher spin bands. The role of this orbital has been discussed in a recent shell-model study across the neutron-rich Cr isotopes [31]. In the current work, the ^{55}Cr data are compared to both collective models and the results of projected shell-model calculations.

II. EXPERIMENT AND DATA ANALYSIS

The experimental method used here is similar to that presented in a number of recent publications [13,21–23,32], and only a summary is given here. A fusion-evaporation reaction with a neutron-rich projectile and target was used to populate yrast and near-yrast states in the two nuclei of interest. A ^{48}Ca^{11+} beam was delivered by the Argonne Tandem Linear Accelerator System (ATLAS). A self-supporting ^{9}Be target of thickness 1.0 mg/cm^2 was used in conjunction with a beam energy of 172 MeV, chosen to optimize $2p$ evaporation. Production cross sections of approximately 10 and 0.1 mb were obtained for the $2n$ channel and the pn channel, producing ^{55}Cr and ^{55}V residues, respectively.

The Gammasphere array [33], containing 101 Compton-suppressed Ge detectors, was used to detect prompt γ decays at the target position. Reaction products were dispersed by the Fragment Mass Analyzer (FMA) [34] according to their mass-to-charge ratio A/q, and their energy-loss characteristics were measured using a segmented-anode ion chamber [35]. Charge-state ambiguities in A/q spectra were overcome using measurements of recoil energy and time of flight, as described in Ref. [13]. The data-acquisition system was triggered by the detection of at least one prompt γ ray in Gammasphere, in coincidence with the arrival of an ion with $A/q = 55/18$ at the focal plane of the FMA, detected by a parallel-plate

gridded avalanche counter located in front of the ion chamber. A total of 1.4×10^8 such events were recorded over a period of 120 h.

The selectivity in A and Z enabled the construction of relatively clean recoil-gated $\gamma\gamma$ coincidence matrices, from which detailed level schemes were constructed. Spin-parity assignments to many of the observed levels in ^{55}Cr were made on the basis of measured angular distributions and directional correlations of oriented states (DCOs). For the former method, experimental data were fitted with the function

$$W(\theta) = A_0 \left[1 + a_2 P_2(\cos\theta) + a_4 P_4(\cos\theta) \right], \qquad (1)$$

where $P_L(\cos\theta)$ are Legendre polynomials and θ is the detector angle relative to the beam direction. For correlation analyses, DCO ratios were deduced as follows. A two-dimensional histogram was incremented when γ rays detected at $\theta = 32°, 37°, 143°, 148°,$ and $163°$ were in coincidence with those detected at $\theta = 79°, 81°, 90°, 99°,$ and $101°$. The DCO ratio is then given by

$$R_{\mathrm{DCO}} = \frac{I_{\gamma_1}^{(\theta_1)} \left[\mathrm{Gate}_{\gamma_2}^{(\theta_2)} \right]}{I_{\gamma_1}^{(\theta_2)} \left[\mathrm{Gate}_{\gamma_2}^{(\theta_1)} \right]}, \qquad (2)$$

where $I_{\gamma_1}^{(\theta_1)}[\mathrm{Gate}_{\gamma_2}^{(\theta_2)}]$ is the intensity of γ_1 detected at θ_1, in a spectrum formed by gating on the DCO matrix at the energy of γ_2 detected at θ_2.

In the case of ^{55}V, statistics were insufficient for full angular distributions or correlations to be measured, so an angular intensity ratio was used, given by

$$R_{\mathrm{ang}} = \frac{\sum_{\theta=79°}^{101°} I_\gamma}{\sum_{\theta=143°}^{163°} I_\gamma}. \qquad (3)$$

Each of these methods was used to ascertain the spin changes associated with γ-ray transitions. These are, in turn, used to propose spin-parity assignments to individual states, in conjunction with yrast-feeding arguments, relative intensities, and other factors, as detailed in the following sections.

III. RESULTS

A. ^{55}Cr

The level scheme for ^{55}Cr deduced in this work is presented in Fig. 1. Transitions were placed according to their coincidence relationships, established from various gated γ-ray spectra, examples of which are found in Fig. 2.

Table I summarizes the observed excitation energies and properties of the γ-ray transitions, along with the measured parameters associated with the angular distributions, which were discussed in the previous section. The scheme consists of several irregular sequences of negative-parity states up to around 3 MeV excitation energy and two regular structures: a single band of positive-parity states on the right-hand side, extending up to a level with a spin of 33/2 at 12226 keV, and two linked bands of negative-parity levels on the left-hand side, reaching a spin of 25/2 at 8015 keV.

The most extensive knowledge of the yrast states for this isotope prior to the present work was deduced using the

^{48}Ca(^{11}B,$p3n$) reaction, as reported in Ref. [2]. Negative-parity states resulting from fp-shell neutron excitations up to $J^\pi = 17/2^-$ were observed, together with a decoupled rotational band up to $J^\pi = 25/2^+$. The present work confirms the existence of most of the γ-ray transitions, with the exception of the tentative 442- and 834-keV lines. Also, the 1744-keV transition that is found feeding the 1439-keV level in Ref. [2] is relocated in the new level scheme. A corresponding 1747-keV transition identified in this work is clearly in coincidence with the 1316- and 1396-keV γ rays [see Fig. 2(b)], and thus, it is placed above these transitions, rather than parallel to them. Consistency checks of energy and intensity sums were used to verify that the current placing of this transition is correct. Extensions have been made to both positive- and negative-parity sequences.

Spins and parities assigned to the levels in Fig. 1 are listed in Table I. Note that only DCO ratios obtained from a gate on the 517-keV transition are listed; ratios obtained from additional gates were also used to verify transition multipolarities.

The spin and parity of the ground state and of the excited states at 242 and 566 keV were adopted from previous studies of the β^- decay of ^{55}V [36] and ^{54}Cr(d,p) and ^{53}Cr(t,p) transfer reactions [37,38]. These data are evaluated and spin-parity assignments are summarized in Ref. [39] and are confirmed by the present measurements.

The regular negative-parity structures to the left of Fig. 1 involve two sequences: one above the ground state and another based on the level at 517 keV, with a series of crossover transitions between them. Although the spin change of every transition is not measured, sufficient information is available from angular distributions and DCO ratios to establish that the sequences are consistent with stretched $E2$ transitions with the crossover transitions being of $\Delta J = 1$ character. Previous polarization measurements of the stronger low-lying transitions [2] indicate that this structure has the same parity as the ground state. Continuation of this sequence and the positive a_2 coefficient for the 2119-keV γ ray suggest a tentative $25/2^-$ assignment to the level at 8015 keV.

In the positive-parity sequence, the $9/2^+$ state at 2085 keV is connected to the 517- and 880-keV $5/2^-$ levels via two parallel pairs of strong transitions, with respective energies of 607 and 961 keV and 871 and 334 keV. Each have a_2 coefficients and DCO ratios, where available, that are consistent with a $\Delta J = 1$ character. The $9/2^+$ state forms the base for a sequence of four transitions, each consistent with spin changes of $2\hbar$. The extension of such a pattern suggests tentative assignments of $29/2^+$ and $33/2^+$ to the states at 9713 and 12226 keV, respectively. The angular distribution of the 2394/2402-keV doublet of transitions is consistent with a similar tentative assignment of $29/2^+$ to the level at 9824 keV. The polarization measurement of Ref. [2] indicates that the 871- and 334-keV transitions have $E1$ and $M1$ character, respectively, resulting in a positive-parity assignment for the state at 2085 keV and, thus, for the sequence above. The same data also fix the multipolarity of the 490-keV line as $E1$, confirming this assignment.

Observed excitation energies of a number of levels without spin assignments are in good agreement with levels predicted
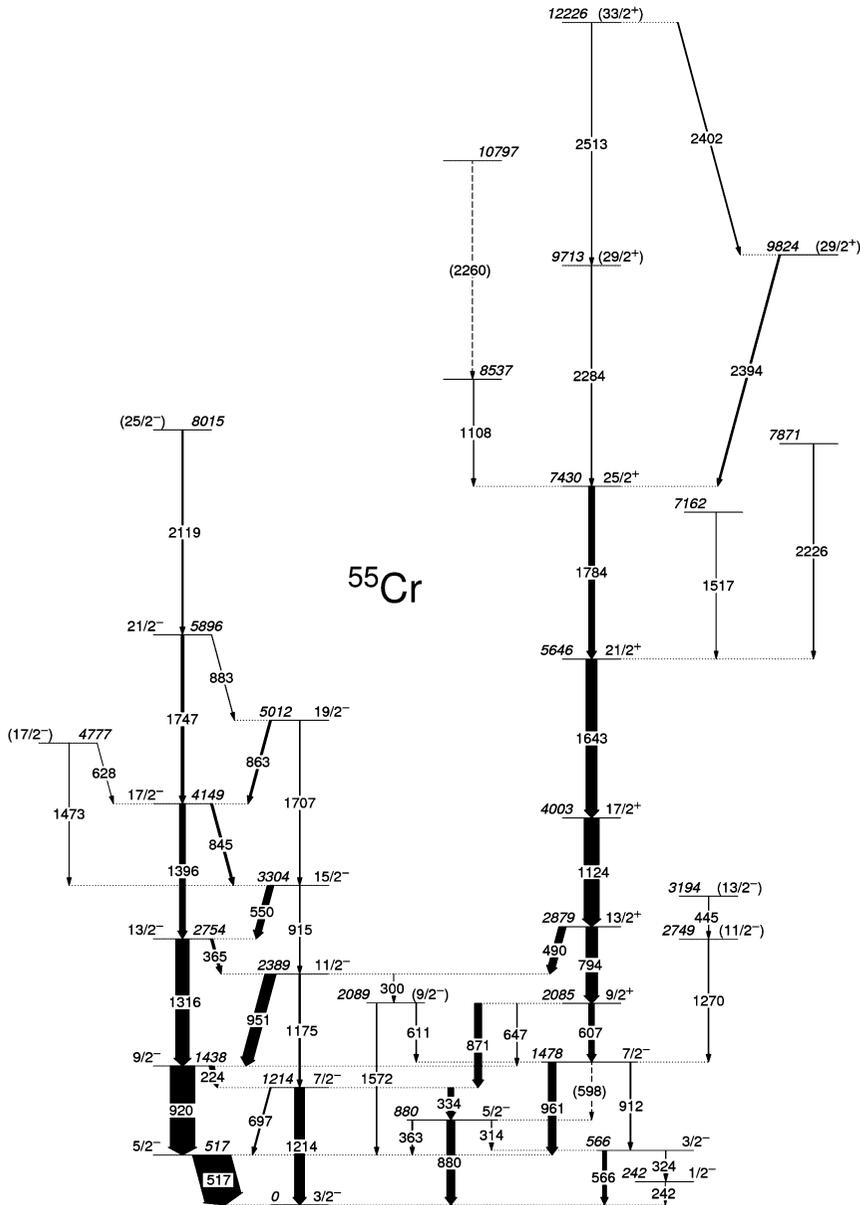
FIG. 1. Level scheme for ^{55}Cr deduced in the present work. Transition and level energies are given to the nearest keV. The widths of arrows are proportional to the relative γ-ray intensities. Tentative assignments and placements are indicated by parentheses and dashed lines.

by shell-model calculations (discussed below), and tentative assignments are proposed on this basis. These include the levels at 3194 and 4777 keV.

B. ^{55}V

A level scheme for ^{55}V, deduced from this work, was previously presented in Ref. [13]. However, the present work provides some revisions to the spin-parity assignments proposed previously, and these are discussed in detail here. In particular, changes have been made to the levels at 4365, 4750, 5171, 5350, 5696, 6621, 7013, and 7467 keV.

The ground-state spin-parity of ^{55}V was established to be $7/2^-$ from β-decay measurements [40]. The level scheme above this state is given in Fig. 3. It exhibits several somewhat irregular sequences of transitions between negative-parity states that extend to a $(19/2^-)$ level at 5039 keV.

Feeding into many of these states are transitions from a series of levels that are tentatively assigned here to be of positive parity, in contrast to the scheme proposed in Ref. [13]. Full details of quantities associated with the levels and transitions in the scheme are given in Table II.

Spin assignments were guided by the angular ratio R_{ang}, as defined above. Pure stretched-dipole transitions are characterized by values of $R_{\mathrm{ang}} > 1$, whereas stretched-quadrupole transitions have $R_{\mathrm{ang}} < 1$. Cases of mixed transitions can lead to some ambiguity, but the presence of many parallel pathways in the ^{55}V decay scheme means that a consistent picture of assignments can be proposed, despite ambiguities for specific individual transitions.

Up to an excitation energy of 2630 keV, spin assignments can be proposed in a relatively straightforward manner, as the experimental indications listed above indicate a stretched character for most transitions. Thus, spin assignments can be proposed and result in an unambiguous overall picture based on
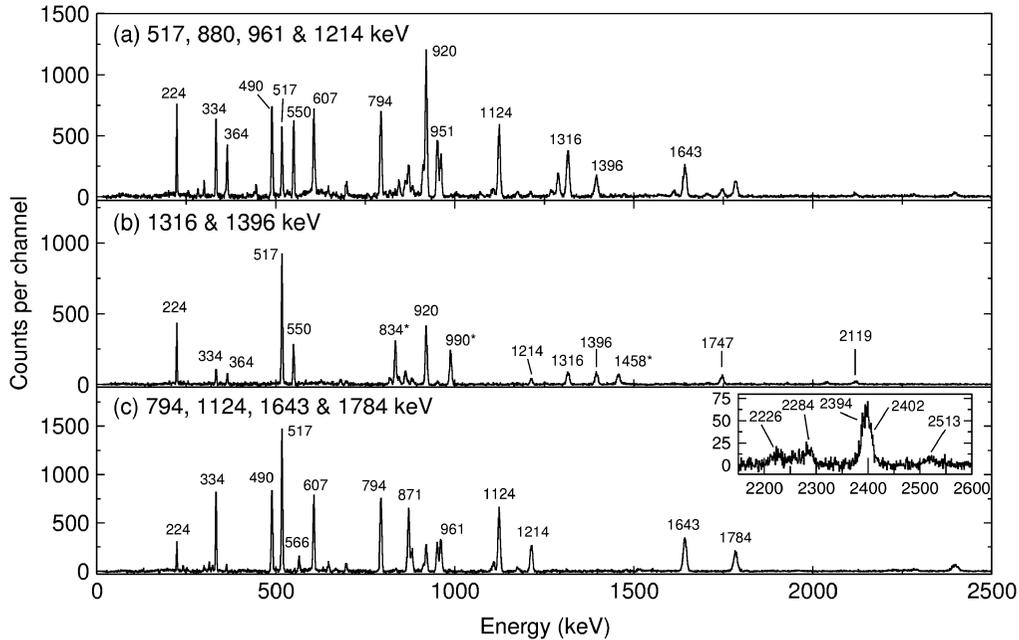
FIG. 2. Spectra obtained from ^{55}Cr-gated $\gamma\gamma$ coincidence events. The energies at which gates were set are indicated within each spectrum; the listed gates have been summed to produce the spectra shown. Peaks are labeled by their energy in keV. Energies marked with an asterisk (*) indicate contaminant peaks from other Cr isotopes. The inset provides a high-energy portion of the spectrum in panel (c), with a magnified intensity scale.

the $7/2^-$ ground state. In this picture, there are two unstretched transitions, both deexciting the level at 2176 keV, with energies of 743 and 234 keV. The former has an angular ratio consistent with unity, whereas the latter is fairly weak. Both run parallel to the 2176- and 606-keV lines, with stretched-quadrupole and stretched-dipole assignments, respectively.

The state at 2643 keV, shown on the right-hand side of Fig. 3, is only fed via a 274-keV γ ray and only deexcites through a 700-keV transition. Although the R_{ang} values, 1.3(2) and 1.4(2), respectively, might indicate stretched-dipole natures, the relatively large errors combined with the lack of corroborating parallel pathways leaves the spin assignment somewhat ambiguous. Further discussion of this state is facilitated by considerations based on shell-model calculations, which will be detailed later.

There are two states at an excitation energy of 1570 keV. Figure 4 provides representative gated γ spectra to confirm the placement of these two levels. Figure 4(a) is the spectrum obtained by gating on the 606-keV transition, which feeds the $9/2^-$, 1570-keV level. There is a prominent photopeak at 1570 keV but not at 1247 keV. The 454- and 606-keV lines are notably absent in Fig. 4(b), which presents the spectrum formed from a gate at 1247 keV. Figure 4(c) is the result of setting a gate at 1621 keV; a slight shift is evident in the main photopeak between Figs. 4(b) and 4(c) due to the 1-keV difference between the γ rays depopulating the 324- and 1943-keV states.

At excitation energies higher than ∼2650 keV, the 4696- and 3479-keV states (found toward the left-hand side of Fig. 3) can be given firm spin assignments based on R_{ang} values. The 2187-keV transition deexciting the 4696-keV level has

an R_{ang} value of 0.5(2), indicating a stretched-quadrupole character and resulting in a $19/2^-$ assignment to the decaying state. The 3479-keV level deexcites to the $11/2_1^-$ state via a 2046-keV transition with $R_{\text{ang}} = 0.8(2)$ and to the $13/2^-$ level at 2630 keV by the 848-keV transition. A picture consistent with yrast feeding arises with a 15/2 spin assignment to the 3479-keV level.

The level at 3165 keV is critical for the spin assignments of most of the levels that lie at higher excitation energies. The 657-keV line has $R_{\text{ang}} = 0.79(4)$, which, at first glance, would suggest a stretched-quadrupole nature but is potentially also consistent with mixed $\Delta J = 0, 1$ cases. Therefore, all three possibilities are considered individually below to assess the most likely spin assignment for the 3165-keV state.

If the 657-keV transition were of stretched-quadrupole character, the state at 3165 keV would be $J^\pi = 19/2^-$. Despite extending the sequence of $E2$ transitions feeding the ground state, this would make the aforementioned 3479-keV level very nonyrast, and it would not be expected to attract such a high level of feeding. This scenario would also result in an $M3$ 534-keV transition deexciting the 3165-keV state, which is unlikely to compete effectively with the 657-keV $\Delta J = 2$ decay. The combination of these arguments leads us to rule out the possibility of the 3165-keV state having a $19/2^-$ assignment.

The hypothesis that the 657-keV line facilitates a spin change of $1\hbar$ leads to an assignment of $J = 17/2$ at 3165 keV. This would still make the 3479-keV state nonyrast, although the 534-keV transition would now be $E2$ in nature.

If the 657-keV γ ray were of $\Delta J = 0$ nature, the 3165-keV state would be $J = 15/2$. The 3479-keV level is

TABLE I. Excited states and transitions in ^{55}Cr, as deduced in the present work. Energies are in keV; intensities are normalized to 100. DCO ratios are those obtained by gating on the 517-keV photopeak. a_2 coefficients listed as <0 or >0 are limits deduced from four-point angular distributions for some of the weaker transitions. Values marked with an asterisk (*) or dagger (†) represent results from unresolved doublets.

E_{level}	J^π	E_γ	I_γ	a_2	a_4	R_{DCO}
242.0(1)	$1/2^-$	241.8(1)	0.75(6)			
517.4(1)	$5/2^-$	517.4(1)	100.0(13)	−0.23(1)		
565.7(1)	$3/2^-$	323.5(1)	0.64(6)			
		565.5(1)	9.6(19)			
880.3(1)	$5/2^-$	314.4(1)	1.4(1)	−0.26(8)		
		362.9(1)	1.8(2)	−0.19(4)*		1.4(4)*
		880.3(1)	21.6(17)			
1214.0(1)	$7/2^-$	333.5(1)	15.1(6)	−0.25(3)		
		696.6(2)	3.2(2)			
		1214.1(1)	26.2(11)	0.16(3)		
1437.7(1)	$9/2^-$	223.5(1)	13.5(4)	−0.30(3)		1.5(6)
		920.4(1)	67.0(21)	0.15(2)	−0.02(2)	1.5(2)
1478.4(1)	$7/2^-$	598.3(2)	0.15(8)			
		912.4(2)	2.3(1)			
		961.0(1)	20.4(8)	−0.36(3)		1.0(2)
2085.0(1)	$9/2^+$	606.5(1)	15.0(5)	−0.28(6)		0.9(2)
		647.0(5)	0.94(10)			
		871.1(1)	19.5(7)	−0.23(3)		
2089.1(2)	$(9/2^-)$	610.6(2)	2.2(2)			
		1572.1(4)	1.6(2)			
2389.1(1)	$11/2^-$	299.9(2)	0.70(6)	<0		
		951.2(1)	29.3(10)	−0.34(2)		0.9(2)
		1175.1(3)	3.6(2)	0.42(6)	−0.28(9)	
2748.9(6)	$(11/2^-)$	1270.4(4)	2.2(2)	>0		
2753.6(2)	$13/2^-$	364.5(1)	6.4(2)	−0.19(4)*		1.4(4)*
		1316.1(1)	36.5(12)	0.18(2)	−0.05(3)	1.8(3)
2878.7(2)	$13/2^+$	489.6(1)	19.2(6)	−0.24(3)		1.0(2)
		793.8(1)	30.9(1)	0.30(2)	−0.04(3)	2.1(6)
3193.9(6)	$(13/2^-)$	445.1(2)	0.81(8)			
3304.2(2)	$15/2^-$	550.4(1)	17.4(6)	−0.30(3)		0.9(2)
		915.3(6)	1.6(9)			
4002.9(2)	$17/2^+$	1124.3(1)	40.5(13)	0.28(2)	−0.08(3)	2.3(4)
4148.9(2)	$17/2^-$	844.6(1)	5.5(2)	−0.61(5)	0.28(6)	
		1395.5(1)	15.3(6)			2.4(5)
4776.9(10)	$(17/2^-)$	627.7(2)	0.16(9)			
		1472.8(8)	0.97(13)			
5011.5(3)	$19/2^-$	862.6(1)	5.4(2)	−0.45(5)		
		1707.1(5)	1.8(2)	>0		
5645.6(3)	$21/2^+$	1642.6(1)	29.5(10)	0.26(3)	−0.11(3)	2.2(5)
5895.5(3)	$21/2^-$	882.8(7)	0.68(13)			
		1746.7(2)	7.3(3)	0.31(5)		2.5(9)
7162.2(6)		1516.6(4)	1.4(1)			
7429.6(3)	$25/2^+$	1784.1(1)	16.5(6)	0.31(4)	−0.12(5)	2.0(6)
7871.3(21)		2225.8(14)	1.2(2)			
8014.8(9)	$(25/2^-)$	2119.2(5)	3.0(2)	>0		
8537.2(6)		1107.6(3)	1.7(1)			
9713.1(15)	$(29/2^+)$	2283.5(10)	1.7(2)	<0		
9823.6(8)	$(29/2^+)$	2393.9(5)	4.3(3)	0.13(7)†	−0.15(10)†	
10797(4)		2260(3)	0.61(16)			
12225.9(16)	$(33/2^+)$	2402.3(10)	2.2(3)	0.13(7)†	−0.15(10)†	
		2512.8(10)	0.8(3)			

then near-yrast, and the 534-keV line has an $M1$ character. An expected $R_{\text{ang}} < 1$ is consistent with the measured value.

Therefore, this assignment appears to be the most probable, and it is the one proposed here.
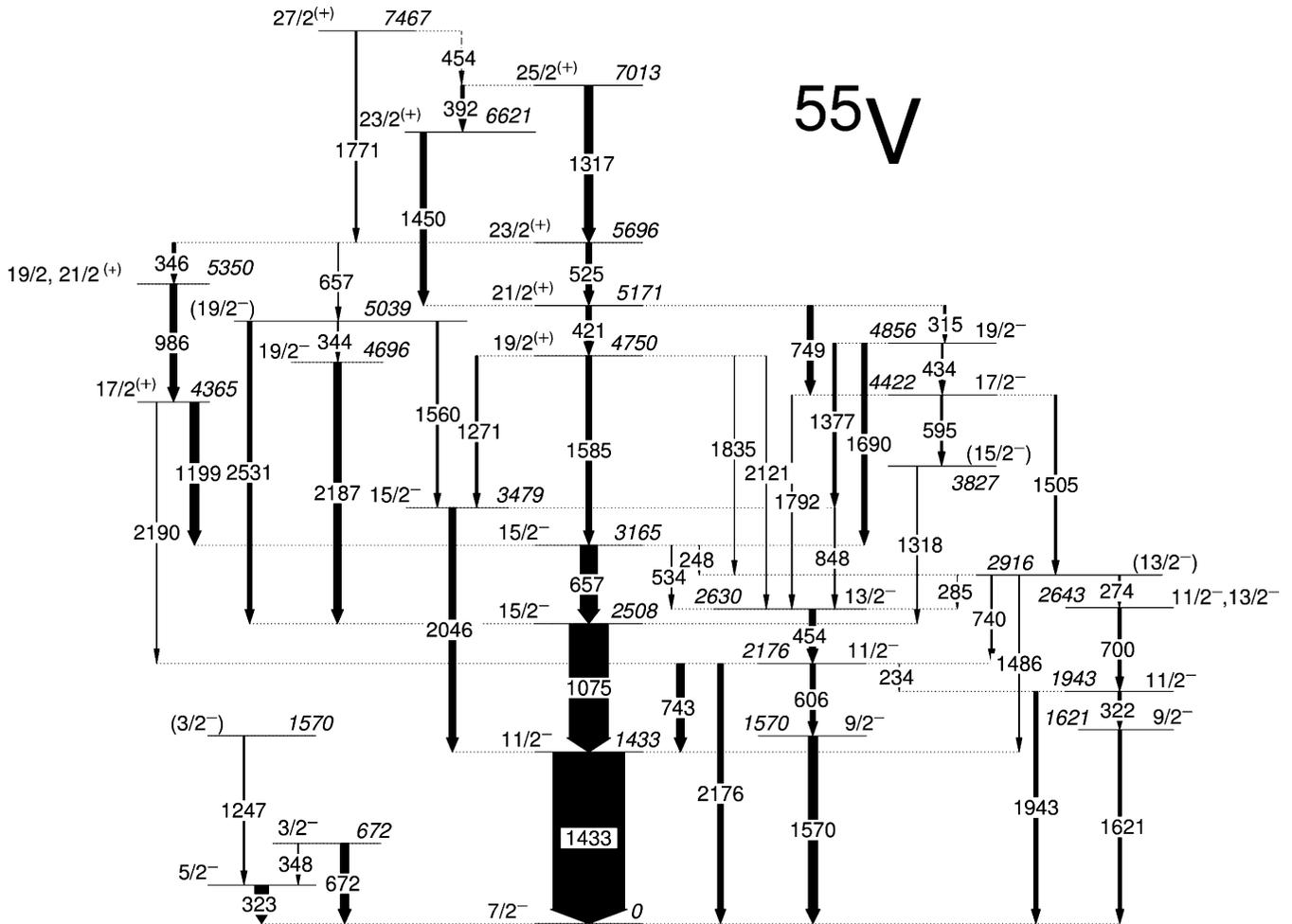
FIG. 3. Level scheme for ^{55}V as deduced in the present work. Level and transition energies are given to the nearest keV. Arrow widths indicate γ-ray intensities. Parentheses and dashed lines indicate tentative assignments and transitions, respectively.

Further weight is given to this scenario by considering the state at 4365 keV, found on the extreme left of Fig. 3. The 1199-keV transition has $R_{ang} = 2.2(4)$, implying a dipole character and, hence, a spin of 17/2 for the 4365-keV level. This state also decays through a 2190-keV γ ray to the $11/2^-$ level at 2176 keV. If the spin of the 3165-keV state were 17/2 or 19/2, this would result in a 4365-keV level with $J = 19/2$ or 21/2, respectively. As a result, the 2190-keV transition would have $\Delta J = 4$ or 5, neither of which is likely to compete effectively with the 1199-keV dipole transition. With the spins as proposed in Fig. 3, the 2190-keV γ ray must have $\Delta J = 3$. Note that this also suggests a positive parity for the 4365-keV level, as the branching ratio is consistent with decay rates expected for an $E3$ transition of 2190 keV.

Arguments similar to those for the 4365-keV level can be applied to the state at 4750 keV, which is displayed in Fig. 3 directly above the low-spin yrast sequence. The 1585-keV γ ray has $R_{ang} = 0.8(3)$, suggesting a spin change of $2\hbar$ and a spin assignment of 19/2 for the 4750-keV level. This state decays via a 2121-keV transition to the 2630-keV level, with a spin already assigned as 13/2. As with the 2190-keV line, a spin change greater than $3\hbar$ is unlikely to result in

an observable intensity for the 2121-keV line, and thus, the assignments of $J = 15/2$ and 19/2 to the states at 3165 and 4750 keV, respectively, are again supported. The octupole nature of the 2121-keV transition also gives the 4750-keV state positive parity, meaning that it decays by two $M2$ and two $E3$ transitions. Such high-multipolarity transitions may suggest that a mixed $\Delta J = 0, 1$ transition is more likely for the 1585-keV line, which would reduce the spin of the 4750-keV state. However, a $\Delta J = 1$ transition can be ruled out on the basis of the measured R_{ang} value. In addition, $\Delta J = 0$ would make the 4750-keV level very nonyrast and would then be inconsistent with the observed feeding intensities. Given the proposed assignment in Fig. 3, with high-multipolarity decays, some consideration should be given to the likely lifetime. A calculation using Weisskopf estimates and $M2$ hindrance factors for this mass region [41] gives a partial half-life of around 50 ps for 1585-keV γ rays. With a recoil velocity of $\sim$0.068c, residues will have traveled $<$1 mm in this time, putting them well inside the target chamber and within the focus of Gammasphere at the time the γ decay takes place. The involvement of higher multipolarities is therefore not inconsistent with the observed intensity. Indeed, there are
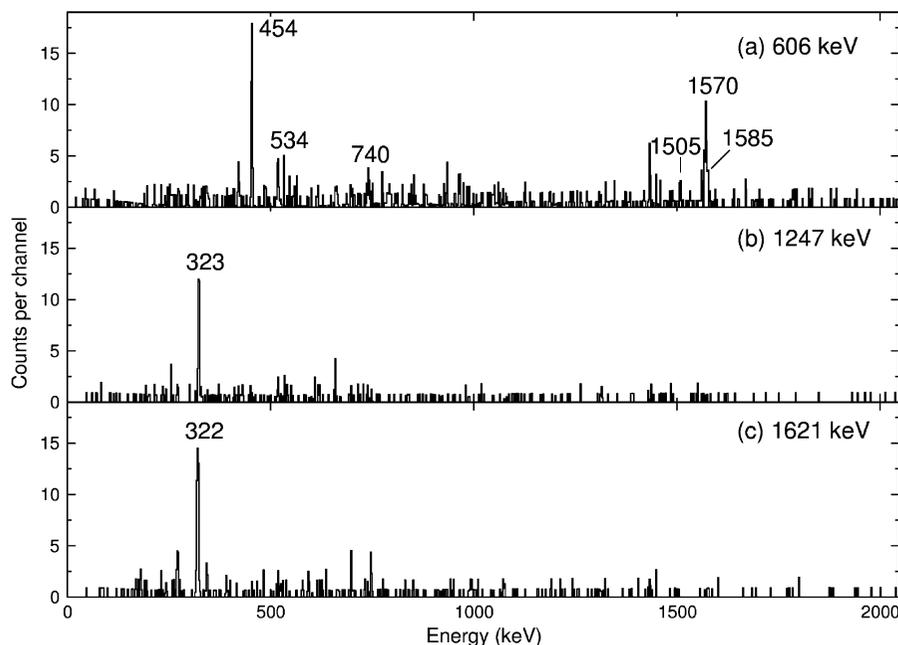
FIG. 4. Gated spectra obtained from a recoil-gated ($A = 55$, $Z = 22$) $\gamma\gamma$ matrix. The energy of the gating transition is given in the top right-hand corner of each panel. Coincident transitions are labeled by their energy in keV.

reasons to expect the presence of $E3$ transitions on the basis of the available single-particle configurations, as discussed in more detail below.

With the assignment of $J = 19/2$ to the 4750-keV state, the spins of the levels above it at 5171, 5696, 6621, and 7013 keV follow from R_{ang} measurements. The 5350-keV level, on the left-hand side of Fig. 3, is restricted to either $J = 19/2$ or $21/2$; both the 986- and 346-keV γ rays have R_{ang} values of a dipole nature, and the states at 4365 and 5696 keV have already been assigned spins of $17/2$ and $23/2$, respectively, on the basis of R_{ang} values. There is clearly some inconsistency here in the experimental information, but it is noted that the ratio for the 986-keV transition, 1.2(1), is rather close to 1.0. Based on yrast feeding arguments, an assignment of $J = 21/2$ is the more likely of the two possibilities above.

The states at 3827, 4422, and 4856 keV on the right-hand side of Fig. 3 have spin assignments fixed by the measured R_{ang} values of the 315-, 595-, 749-, and 1690-keV transitions. However, the spin of the 3827-keV level is given as tentative due to the large error on the R_{ang} value and the absence of other decay paths to confirm the assignment of $15/2$. Below these transitions in Fig. 3, the state at 2916 keV is given a tentative assignment of $J^{\pi} = 13/2^{-}$. This is based on the R_{ang} values determined for the 274- and 1505-keV γ rays. The former has $R_{ang} = 1.3(2)$, consistent with $\Delta J = 0, 1$; the latter, with $R_{ang} = 1.1(1)$, indicates $\Delta J = 0, 1, 2$. The combination of these, along with yrast feeding arguments and the presence of transitions from states with firmly established spins, suggests that $13/2$ is the most likely assignment for this level.

IV. DISCUSSION

A. Shell-model calculations

Shell-model calculations were performed for the two nuclides using three effective interactions in the full fp model space: KB3G [42], GXPF1A [12], and GXPF1B [14]. The latter two interactions are of the same generic type. Only negative-parity experimental states can be compared with calculated levels in these calculations; positive-parity states are indicative of excitations across $N = 40$ and involve a larger model space. In order to address a wider space within a shell model and describe collective structures, projected shell-model (PSM) calculations were performed for ^{55}Cr. In this approach, a deformed quasiparticle basis deduced from a Nilsson-BCS model is used, and angular momentum projection is carried out to form shell-model configurations in the laboratory frame. Configuration mixing is performed as in traditional shell-model calculations, but now in a much smaller projected basis rather than in a large spherical shell-model one [27]. Such calculations have recently been able to describe collective structures in neutron-rich even Cr and Fe isotopes [28,29].

1. ^{55}Cr

The calculated levels for ^{55}Cr are compared with the negative-parity experimental states in Fig. 5, where, for clarity, only the two lowest ones of each spin are given for the calculations.

The overall structure of the negative-parity states is fairly well reproduced by all three traditional shell-model calculations, but they differ in a detailed comparison, with the two GXPF1 calculations reproducing the order of the experimental levels slightly better than the KB3G results. The root-mean-square (rms) deviations between each prediction and the experimental levels are given in Table III.

Values are quoted for two cases: the first includes only states with unambiguous experimental spin and parity assignments, whereas the second takes all proposed negative-parity experimental states into account. This more detailed comparison indicates a level of improvement in the GXPF1 family of
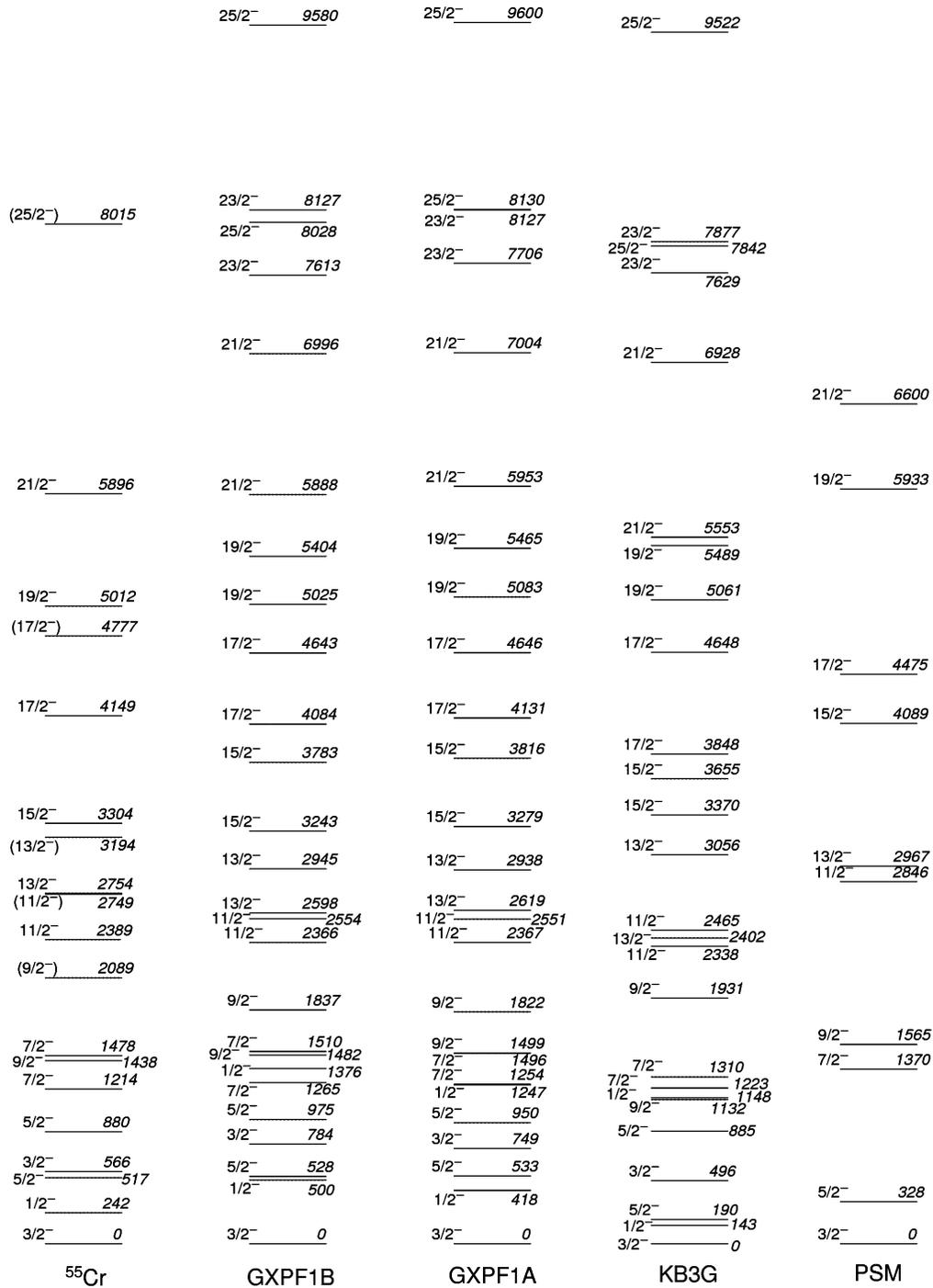
FIG. 5. Negative-parity experimental levels in ^{55}Cr compared to results of calculations using the KB3G, GXPF1A, and GXPF1B interactions and the projected shell model (PSM) (see text for details). Only the lowest two calculated states of each spin are shown, except in the case of the PSM calculations, where only the yrast states are provided. Level energies are given to the nearest keV.

interactions compared to the KB3G interaction for ^{55}Cr, particularly in the reproduction of states with firm assignments. The refinements incorporated in GXPF1B do not seem critical, at least for the subset of states populated in this experiment.

A number of tentative spin-parity assignments are suggested by the comparison of experimental and calculated levels. For example, it can be seen in Fig. 5 that the $13/2_2^-$

and $17/2_2^-$ states, predicted at energies of 2938 and 4646 keV by the GXPF1A calculations, provide reasonable shell-model counterparts for the two experimental states at 3194 and 4777 keV. Note that these two states are also reproduced in a similar way in calculations with the GXPF1B and KB3G interactions. These experimental states are tentatively assigned $J^\pi = 13/2^-$ and $17/2^-$, respectively, on this basis. These

TABLE II. Excited states and transitions in ^{55}V, as deduced in the present work. Energies are in keV; intensities are normalized to 100. Details about the extraction of the angular ratio R_{ang} are given in the text.

E_{level}	J^{π}	E_{γ}	I_{γ}	R_{ang}
323.8(3)	$5/2^-$	323.1(5)	19.2(21)	1.2(1)
671.9(2)	$3/2^-$	347.9(3)	1.4(10)	
		672.0(2)	11.5(15)	0.9(1)
1433.1(1)	$11/2^-$	1433.1(1)	100(6)	0.77(5)
1570.0(3)	$9/2^-$	1569.7(4)	13.3(21)	1.5(2)
1570.4(6)	$(3/2^-)$	1246.6(5)	2.0(15)	2.5(1.4)
1620.8(4)	$9/2^-$	1620.8(8)	4.5(9)	1.2(1)
1942.8(3)	$11/2^-$	322.0(3)	4.5(15)	
		1943.2(7)	5.8(11)	0.73(5)
2176.4(2)	$11/2^-$	233.8(5)	0.50(20)	
		606.3(2)	6.9(8)	1.7(4)
		742.9(4)	10.7(13)	1.1(1)
		2175.5(10)	8.1(23)	0.8(2)
2508.1(1)	$15/2^-$	1075.0(1)	54(3)	0.79(3)
2630.2(3)	$13/2^-$	453.8(1)	8.8(8)	1.6(1)
2642.6(3)	$11/2^-, 13/2^-$	699.9(3)	4.5(7)	1.4(2)
2916.3(3)	$(13/2^-)$	273.7(1)	2.5(3)	1.3(2)
		285.1(5)	0.5(3)	
		739.9(7)	2.5(12)	
		1486.4(9)	1.2(7)	
3165.4(2)	$15/2^-$	248.2(12)	0.6(3)	
		534(4)	0.5(3)	
		657.4(1)	24.2(10)	0.79(4)
3479.2(6)	$15/2^-$	848.1(11)	1.4(9)	
		2046.2(13)	9.9(15)	0.8(2)
3826.8(6)	$(15/2^-)$	1318.3(13)	1.0(5)	
4364.6(5)	$17/2^{(+)}$	1199.0(5)	12.3(8)	2.2(4)
		2190.4(22)	0.5(3)	
4421.7(4)	$17/2^-$	594.8(5)	3.3(8)	1.7(5)
		1505.0(7)	3.3(8)	1.1(1)
		1791.7(11)	1.1(8)	
4695.5(9)	$19/2^-$	2187.4(10)	10(3)	0.5(2)
4750.2(4)	$19/2^{(+)}$	1270.6(7)	3.3(12)	
		1584.7(5)	8.1(8)	0.8(3)
		1835.4(12)	0.5(3)	
		2121(3)	0.5(3)	
4855.7(4)	$19/2^-$	433.9(5)	2.4(9)	
		1376.9(12)	4.7(16)	
		1690.2(9)	7.1(6)	0.6(3)
5039.1(9)	$(19/2^-)$	343.6(4)	1.5(7)	
		1560(3)	2.8(12)	
		2531.0(24)	6(2)	
5170.8(4)	$21/2^{(+)}$	315.1(1)	3.8(5)	1.2(1)
		420.6(1)	7.2(7)	1.6(1)
		748.5(10)	8.2(12)	0.76(8)
5350.2(5)	$19/2, 21/2^{(+)}$	985.6(3)	9.7(11)	1.2(1)
5695.8(4)	$23/2^{(+)}$	345.7(10)	4.9(9)	1.5(3)
		525.0(1)	7.8(8)	1.4(1)
		657(4)	1.0(5)	
6620.6(4)	$23/2^{(+)}$	1449.8(3)	8.9(12)	1.3(2)
7012.6(4)	$25/2^{(+)}$	392.0(1)	4.6(5)	1.6(2)
		1316.9(4)	11.9(14)	1.0(1)
7466.8(9)	$27/2^{(+)}$	454.1(10)	0.10(10)	
		1771.0(15)	2.3(11)	0.9(3)

TABLE III. The rms deviations between calculated and experimental levels in ^{55}Cr and ^{55}V. Values are given to the nearest keV for the cases of all negative-parity experimental levels and for those with firm spin-parity assignments only; values for ^{55}V are also given for the first two levels of each spin for a more consistent comparison with ^{55}Cr.

Isotope	Levels included	GXPF1B	GXPF1A	KB3G
^{55}Cr	All negative-parity levels	138	131	205
	Firm J^{π} assignments only	112	89	212
^{55}V	All negative-parity levels	304	276	256
	Firm J^{π} assignments only	271	263	233
	First two levels of each spin	223	210	258

assignments also appear to be consistent with the expected yrast feeding and γ-ray intensities.

There is a regular structure composed of two sequences of $E2$ transitions connected by crossover γ rays based on the ground state of ^{55}Cr on the left-hand side of the experimental level scheme (Fig. 1). At first glance, this is somewhat suggestive of the two signatures of a coupled rotational band. However, this structure can be adequately described within the GXPF1 shell-model calculations. The energies of the levels in this sequence are well reproduced with a low rms deviation in the comparison with experiment (68 keV). This is in contrast to the KB3G interaction, where the ordering of levels is not reproduced as well. In addition, there is a tendency to underestimate their excitation energies. The comparison between the GXPF1 calculations and experiment goes further than the excitation energies, with reasonable reproduction of the pattern of γ decays between levels in this structure, as discussed below.

The crossover transitions between states in the two $E2$ sequences appear to be predominantly $M1$ in nature. Transition rates calculated using the GXPF1 interactions indicate mixing ratios with values less than 0.1. The angular distributions measured for most of the transitions have large and negative a_2 coefficients, with no indication of any a_4 influence that might have indicated $E2$ admixtures. The 845-keV transition connecting the states at 4149 and 3304 keV is an exception, having a measured a_4 coefficient greater than zero, although statistically significant mixing ratios could not be extracted from the data. The 697- and 883-keV transitions were too weak to obtain reliable angular distributions.

A comparison of the experimental and calculated branching ratios for the "in-band" $E2$ transitions is presented in Table IV. For the yrast $9/2^-$, $13/2^-$, $17/2^-$, and $21/2^-$ states, the branch via the $E2$ transitions is high and fairly constant around 75%. The calculated GXPF1A wave functions for these states are dominated by a $\pi f_{7/2}^4 \nu f_{7/2}^8 p_{3/2}^2 f_{5/2}^1$ configuration, while other configurations for these states have probabilities <10%. The fraction of the dominant configuration increases with spin, from 38% in the $5/2^-$ state to 61% in the $25/2^-$ level. The calculated branching ratios are also fairly constant throughout the sequence, albeit somewhat overestimated compared to the experimental numbers. The reproduction of the second sequence of states with spins $3/2^-$, $7/2^-$, $11/2^-$, $15/2^-$, and

TABLE IV. Calculated and experimental branching ratios for the $E2$ transitions out of states forming the regular negative-parity bands in ^{55}Cr (see text for details).

State	$E2$ Branching Ratio	
	GXPF1A	Experiment
$21/2^-$	90%	79(10)%
$17/2^-$	90%	72(6)%
$13/2^-$	97%	78(4)%
$9/2^-$	88%	74(2)%
$15/2^-$	56%	7(2)%
$11/2^-$	36%	4(1)%
$7/2^-$	66%	42(22)%

$19/2^-$ is less satisfactory, but the structure is more complex. These have a dominant $\pi f_{7/2}^4 \nu f_{7/2}^8 p_{3/2}^3$ configuration, although the importance of other admixtures is increased and changes with spin. For example, the $\pi f_{7/2}^4 \nu p_{3/2}^2 f_{5/2}^1$ configuration becomes more significant for the $7/2_1^-$ and $19/2_1^-$ levels with probabilities of 12% and 18%, respectively. It should be noted that the experimental $7/2^-$ and $11/2^-$ states have additional branches to other parts of the level scheme (see Fig. 1) and, as such, are likely to be more difficult to reproduce theoretically.

Overall, the comparison of excitation energies and branching and mixing ratios for this regular structure between the data and the GXPF1 calculations appears to give a reasonable reproduction of the pattern of γ decays. More generally, the predictions of the different calculations for ^{55}Cr appear to favor the GXPF1 family of interactions. This conclusion agrees with those found in work on other nuclei in the neutron-rich fp shell, where the success of the GXPF1-type interactions are well documented in Sc, Ti, Cr, and Mn isotopes, although limitations at high spin and in the more neutron-rich Mn and Cr nuclei have been noted [13,21,22,30,43,44]. With this general success in the region, there is clearly a strong impetus to test the GXPF1A predictions of the presence of a $N = 34$ gap in ^{54}Ca.

The results of the PSM calculations are presented in comparison with experimental energy levels in Fig. 5 for negative-parity states and in Fig. 6 for the high-spin positive-parity sequence. In both cases, only the lowest calculated state for each spin is given. It is no surprise that the comparison with the low-lying negative-parity states is worse than in the traditional shell-model approaches. The basis used by the PSM was generated at a deformation of $\varepsilon_2 = 0.21$, and a much larger space would be required to describe the spherical low-lying states to the degree of accuracy achieved in the conventional shell-model approaches. However, the PSM calculations are quite successful in reproducing the pattern of positive-parity states, as indicated by the comparison in Fig. 6. The structure of the calculated sequence is dominated by a decoupled $K = 1/2$ band based on a neutron $g_{9/2}$ excitation; the $1/2^+$ and $5/2^+$ states are predicted to lie higher in excitation energy than the apparent $9/2^+$ bandhead, consistent with their nonobservation in the experimental data. Beyond a spin of $25/2$, the calculations predict that this structure is crossed by a three-quasiparticle band consisting of a $K = 1/2$ neutron

^{55}Cr	PSM
$(29/2^+)$ 9824	
$(29/2^+)$ 9713	$29/2^+$ 9298
$25/2^+$ 7430	$25/2^+$ 7151
$21/2^+$ 5646	$21/2^+$ 5441
$17/2^+$ 4003	$17/2^+$ 4028
$13/2^+$ 2879	$13/2^+$ 2765
$9/2^+$ 2085	$9/2^+$ 1881
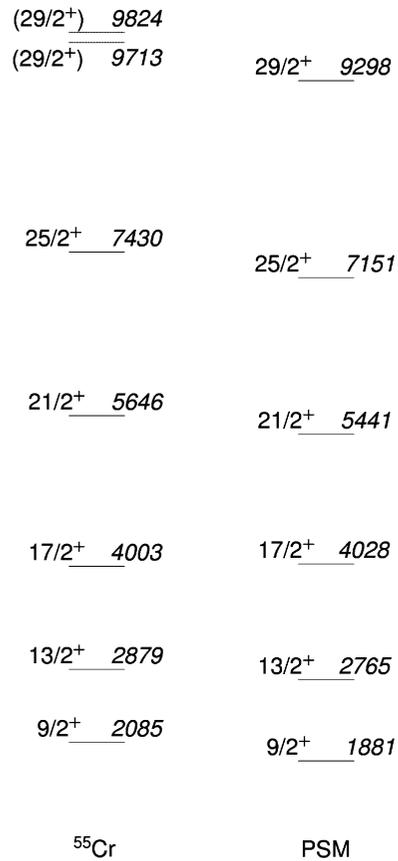
FIG. 6. PSM calculations for the positive-parity band in ^{55}Cr in comparison with the data. Level energies are given to the nearest keV. See text for details.

with a $g_{9/2}$ spherical parentage and two protons in $K = 3/2$ and $K = 5/2$ Nilsson states arising from the $f_{7/2}$ state. It is interesting to note that two separate decay paths are observed to feed the $25/2^+$ state at 7430 keV (see Fig. 1), and it is intriguing to speculate that the two tentative $29/2^+$ states at 9713 and 9824 keV correspond to these two different configurations in the region where they are both near yrast.

2. ^{55}V

The results of shell-model calculations for ^{55}V with the same three interactions used for ^{55}Cr are displayed alongside the negative-parity experimental levels in Fig. 7.

In this case, the number of calculated states plotted at each spin is the same as experimentally observed; additional calculated levels with no experimental counterparts are not shown for clarity. It is important to note that a far greater number of nonyrast states were populated in ^{55}V than in ^{55}Cr, and so caution is necessary when comparing the two nuclides. In order to make a fair comparison, an additional set of rms deviations are quoted for ^{55}V in Table III, calculated only for the lowest two states of a given spin.

As is the case with ^{55}Cr, the calculations from all three interactions reflect the general distribution of experimental levels. However, as indicated in Table III, while the KB3G interaction
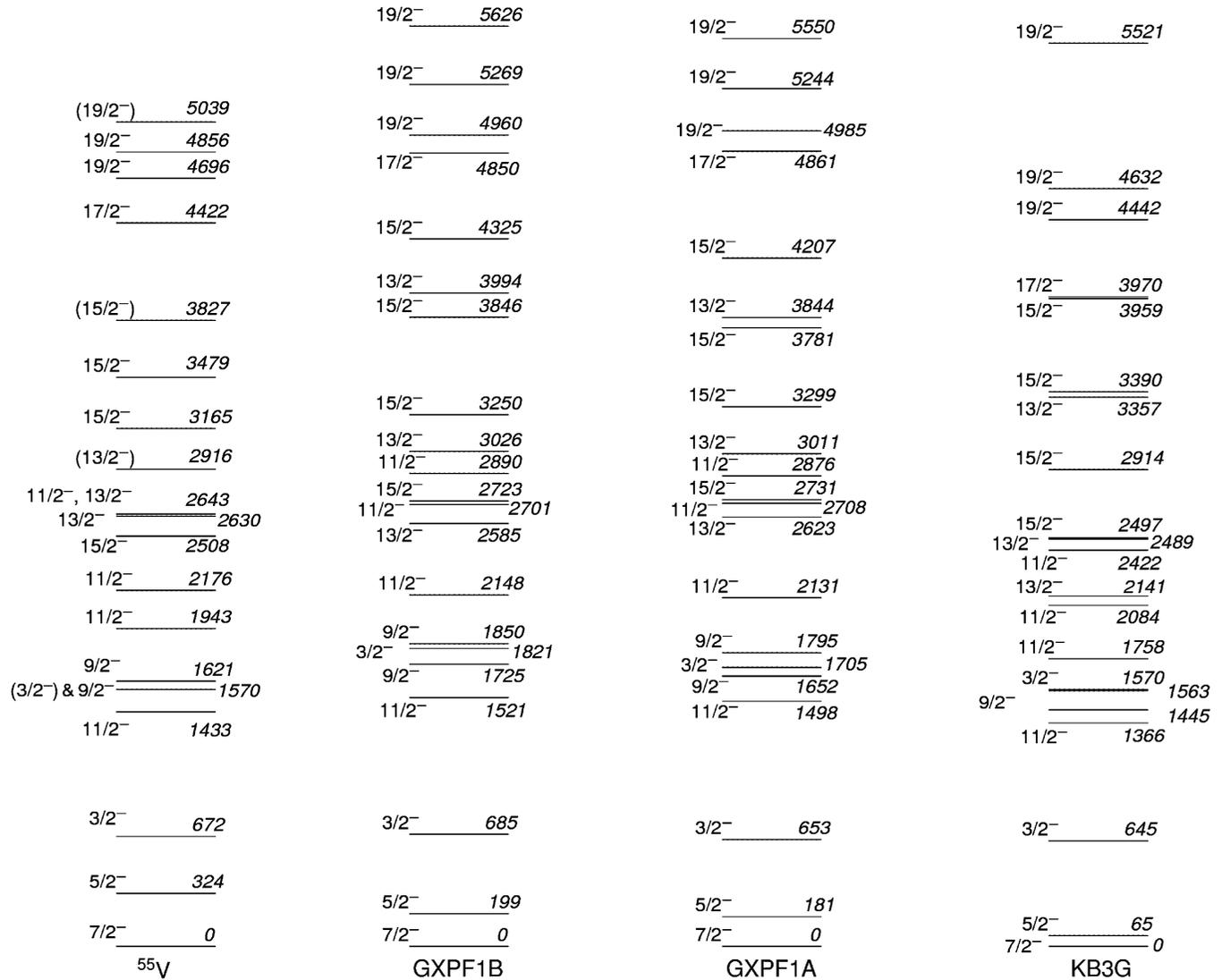
FIG. 7. Negative-parity experimental states in ^{55}V compared to results of shell-model calculations with the GXPF1A, GXPF1B, and KB3G interactions (see text for details).

results in a similar rms deviation from the experimental levels as in ^{55}Cr, this does not improve significantly with either of the newer GXPF1 interactions. The three interactions produce a reasonable agreement with the low-lying levels. Large energy differences emerge above 2 MeV, along with some reordering of the energy levels.

The 324-keV experimental state, also observed in the β decay of ^{55}Ti [40], is placed 259, 143, and 125 keV too low by calculations with the KB3G, GXPF1A, and GXPF1B interactions, respectively, while the observed $3/2_1^-$ level lies within 27 keV of all three theoretical counterparts. The nonyrast state observed experimentally at 1570 keV is given a tentative spin-parity assignment of $3/2^-$ on the basis of the shell-model calculations. The GXPF1A interaction predicts a $1/2^-$ level at 1660 keV and a $3/2^-$ state at 1705 keV. Though the $1/2^-$ level is closer in energy to 1570 keV, it would be so nonyrast that observation in this work is highly unlikely. The measured R_{ang} value for the 1247-keV transition also indicates a dipole nature. An estimate of transition rates for

$M1$ and $E2$ γ rays of this energy, using enhancement factors for this mass region [41], suggests that an $E2$ transition should have around 100 times the intensity of the $5/2^- \rightarrow 7/2^-$ line that feeds the ground state, whereas the $M1$ transition rate is consistent with the measured intensity of the 1247-keV γ ray.

The experimental state at 2643 keV has been limited to a spin of $11/2$ or $13/2$, as discussed in Sec. III B. However, comparison with shell-model calculations favors the former. If a spin of $13/2$ is adopted for this level, the experimental state at 2916 keV, also tentatively assigned $J^\pi = 13/2^-$, would have its theoretical counterparts at 3357, 3844, and 3994 keV in the KB3G, GXPF1A, and GXPF1B interactions, respectively. This, in turn, would result in rms deviations between all experimental levels and the calculations of 254, 354, and 397 keV, respectively. While this is a slight (2 keV) decrease for the KB3G interaction, it represents increases of 21 and 40 keV for the deviations from the two GXPF1 interactions. Due to these inconsistencies between the

three interactions, this particular spin assignment remains uncertain.

For the highest-energy negative-parity states, further break-down emerges in the agreement between theory and experimental levels. While the KB3G interaction places the $17/2_1^-$ level around 500 keV too low in energy, both GXPF1 interactions put it around 400 keV too high.

The conclusions discussed in our previous publication [13], where comparisons were made to calculations with the GXPF1A interaction only, still stand and are summarized briefly here. ^{55}V can be viewed as a single proton outside ^{54}Ti, a nucleus exhibiting aspects of shell stability due to the gap in the neutron single-particle structure at $N = 32$ [4]. This is illustrated by noting the similarity in excitation energy between the lowest-lying $11/2^-$ and $15/2^-$ states at 1433 and 2508 keV in the former, dominated by recoupling of the $f_{7/2}^3$ proton with the 2_1^+ and 4_1^+ states in the latter at 1495 and 2508 keV, generated by the $\pi f_{7/2}^2$ configuration. Excited states at low energy are generated by the promotion of at least one neutron to a $p_{1/2}$ or $f_{5/2}$ state, and they exhibit a high degree of mixing due to the close proximity of these orbitals. The decay of the $15/2_2^-$ state at 3165 keV to a state of the same spin at 2508 keV, rather than the lower $11/2_1^-$ level, is understood as resulting from the differences in structure. The decay of the $15/2_2^-$ state dominated by a $[\pi f_{7/2}^3 \otimes f_{7/2}^8 p_{3/2}^3 f_{5/2}]_{15/2^-}$ configuration to the $11/2_1^-$ state requires a change in neutron configuration and a recoupling of proton spin, whereas the observed decay pathway only requires the former.

The re-evaluation of the spin-parity assignments presented in the current work for states above 4 MeV in excitation energy has highlighted the importance of high-energy $E3$ transitions in the decay of high-lying positive-parity levels that compete effectively with lower-energy $M2$ and $E1$ decays. Given that the positive-parity levels are likely to have contributions from $g_{9/2}$ neutrons, the appearance of the octupole decays is likely to be driven by the availability $\Delta \ell = 3$, $\Delta j = 3$ transitions between $g_{9/2}$ and $p_{3/2}$ neutron orbitals.

The inclusion of $g_{9/2}$ neutrons into the model space is only one issue that complicates shell-model approaches. Both one- and two-proton knockout reactions from ^{54}Ti have indicated the importance of proton sd-shell contributions in ^{53}Sc [45] and ^{52}Ca [43] at a few MeV excitation. It is, therefore, likely that sd-fp cross-shell excitations are involved in the wave functions of states at high excitation in ^{55}V. Similar conclusions have been drawn about highly excited states populated in ^{51}Ca and ^{52}Sc [16]. A suitable proton effective interaction for cross-shell excitations is currently missing. Indeed, the situation appears to be similar to that in the $A = 30$ region near the island of inversion where measurements of excited states have highlighted the inadequacies in the current shell-model descriptions of cross-shell proton excitations, even when they occur at relatively low energy [46,47].

B. Intruder configurations and collectivity

As already argued above, the positive-parity states observed in both isotopes must arise from particle-hole cross-shell excitations. Such configurations, most likely involving
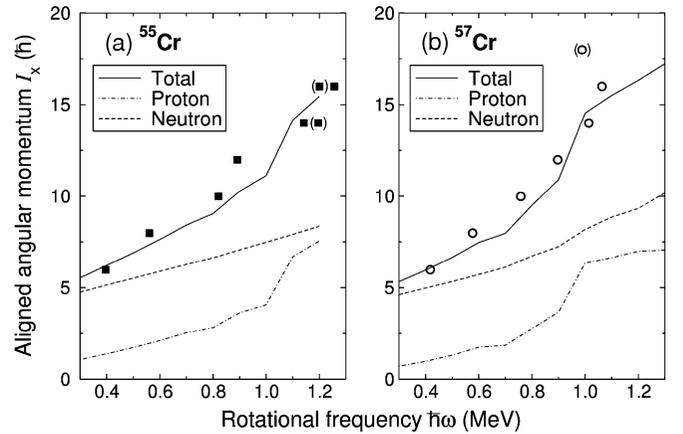
FIG. 8. Experimental and calculated aligned angular momenta along the rotation axis I_x, as a function of rotational frequency, for positive-parity states in (a) ^{55}Cr and (b) ^{57}Cr. Data points in parentheses indicate the alternative decay path in ^{55}Cr ($E_\gamma = 2402$ and 2394 keV) and the tentative 1978-keV transition in ^{57}Cr (see text and Ref. [22] for details). Note that both plots are given with the same x and y scales to aid comparison.

the $\nu g_{9/2}$ orbital, have been observed across the neutron-rich fp-shell nuclides [13,21,22,32,44]. In many cases, the positive-parity states form regular quasirotational bands, often extending to spin values approaching termination of the $\nu g_{9/2}$ configurations involved. This is consistent with the ^{55}Cr findings presented here. However, unlike in recent work on its more neutron-rich neighbors $^{56-60}$Cr, the assignment of positive parity to these states is not based on systematics or spin assignments beyond the maximum possible in a $\nu(f_{5/2}p_{3/2}p_{1/2})^{N-28}$ configuration. Rather, the positive parity of the 2085-keV level is known through a previous study [2] in which polarization coefficients were measured for the 490- and 871-keV deexcitation transitions, thus unambiguously determining their $E1$ character. The fact that the present work observes this positive-parity band up to spin 33/2, the maximum allowed for a $\nu g_{9/2}$ configuration, adds weight to arguments that this is the orbital involved in the excitation. Furthermore, the observation of a single signature of a quasirotational band suggests a low-Ω configuration, such as $1/2^+[440]$, leading to a high degree of decoupling, and a rotation-alignment scheme favored with prolate deformation. These arguments have been presented in detail in Ref. [22], where a very similar structure has been observed in ^{57}Cr. Indeed, Ref. [22] compared the aligned angular momenta for the positive-parity states in ^{55}Cr and ^{57}Cr, using the data available from Ref. [2]. This picture can now be extended with the new results presented in Fig. 8. Total-Routhian-surface (TRS) calculations were performed, using the "universal" set of Woods-Saxon parameters from Ref. [48] and the diabatic blocking procedures described in Ref. [49], in order to show consistency with the suspected prolate deformation associated with the positive-parity band. The experimental aligned angular momentum is presented as a function of rotational frequency for the quasirotational bands in ^{55,57}Cr in Fig. 8, along with predictions from TRS calculations.
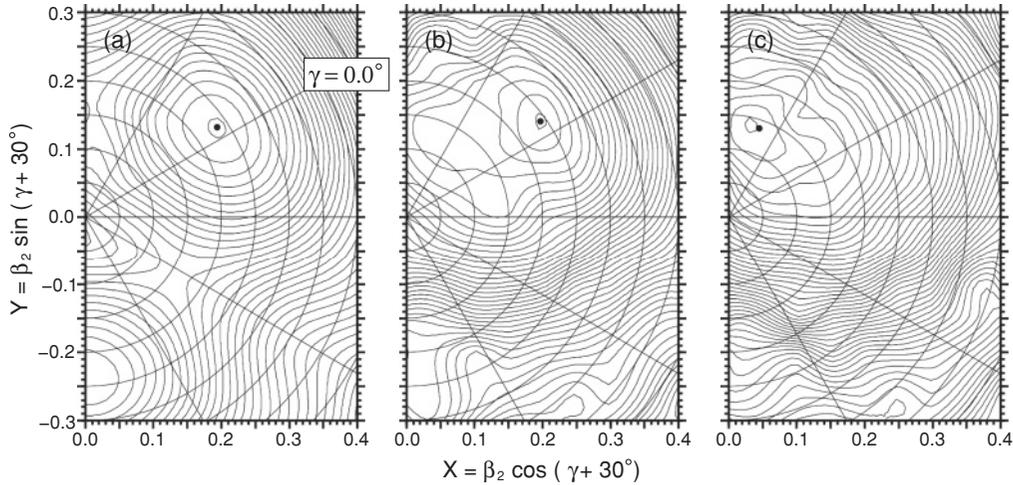
FIG. 9. Total-Routhian-surface plots for ^{55}Cr, with protons in their vacuum configuration and the valence neutron occupying the lowest-lying $\Omega^\pi = 1/2^+$ orbital at the following angular frequencies: (a) $\hbar\omega = 0.2$ MeV, (b) $\hbar\omega = 1.0$ MeV, and (c) $\hbar\omega = 1.4$ MeV. A dot represents the absolute minimum in each plot, and contours are shown at 200-keV intervals.

Interpretation of the data for ^{55}Cr is somewhat dependent on which decay path is chosen for the two transitions at the top of the band. The 2513- and 2284-keV transitions populate and deexcite, respectively, the yrast $29/2^+$ state at 9713 keV and lead to a smooth continuation of the data points to the highest rotational frequencies in Fig. 8. However, a parallel pathway exists via the 2402- and 2394-keV transitions. The $29/2^+$ state lies at 9824 keV and is, therefore, over 100 keV nonyrast compared to the former decay route. Despite this, the nonyrast path experiences the greater feeding of the two, with the transitions being around twice as strong as their parallel counterparts. These more intense transitions lead to the two ^{55}Cr data points in parentheses in Fig. 8 and would, therefore, indicate a sharp discontinuity in the aligned angular momentum of the band around $\hbar\omega = 1.2$ MeV. The calculations suggest that the bands in both isotopes should exhibit an upbend, as a result of a proton alignment, around $\hbar\omega = 1$ MeV, albeit at a slightly higher rotational frequency in ^{55}Cr than in ^{57}Cr. The experimental data support the presence of such an alignment, although the upbend in ^{55}Cr is not delineated well, with the two possible decay paths and the fact that $J^\pi = 33/2^+$ corresponds to termination for a $\nu(f_{5/2}p_{3/2}p_{1/2})^2(g_{9/2})^1$ configuration.

Potential-energy surface calculations for ^{55}Cr can be found in Fig. 9. In the case of the ground-state configuration (*not* shown in Fig. 9), a rather shallow minimum exists near $\beta_2 = 0.20$ and $\gamma \approx 0°$. Figures 9(a), 9(b), and 9(c) represent tracked TRS calculations based on the lowest-lying $\Omega^\pi = 1/2^+$ configuration. Figure 9(a) is calculated at rotational frequencies toward the lower part of the positive-parity band of Fig. 1. In this case, a well-defined prolate minimum occurs with deformation parameters $\beta = 0.24$ and $\gamma \sim 0°$, implying an approximately axially symmetric nuclear shape. The increase in β_2 relative to the ground-state configuration can be attributed to the deformation-driving effect of the $\nu g_{9/2}$ intruder orbit. Figures 9(b) and 9(c) illustrate the

situation for intermediate and "high" rotational frequencies within the quasirotational band. The movement in the position of the minimum away from the collective prolate axis at $\gamma = 0°$ toward the noncollective oblate axis at $\gamma = 60°$ is characteristic of the phenomenon known as "smooth" band termination [50,51]. In this interpretation, the deformation associated with the configuration giving rise to the collective structure in the low-spin regime gradually shifts toward the $\gamma = 60°$ noncollective axis as the spins of the valence nucleons and holes gradually align along the axis of rotation. Such trends are well documented for nuclei in the $A \sim 110$ mass region [52].

It is interesting to compare the results of TRS calculations for the $g_{9/2}$ band in ^{55}Cr with those of ^{57}Cr (see Fig. 3 of Ref. [22]). As the corresponding band in ^{57}Cr is also observed up to a spin consistent with termination of the $\nu g_{9/2}$ configuration, it may be expected that the TRS plots take on similar characteristics. While this is true for lower rotational frequencies, the results differ as termination is approached. In ^{57}Cr, the absolute minimum remains near $\gamma = 0°$, shifting toward $\beta_2 = 0.1$, while the spacing between contours increases, indicating a fairly flat energy surface.

The positive-parity states in ^{55}V do not provide such an immediate physical interpretation. In this case, the overall structure seems to be much less well defined. This is consistent with the expectation that collective positive-parity sequences may not be well developed at the $N = 32$ subshell closure. In comparing ^{55}V with ^{55}Cr, it appears that the addition of a proton may enable a softness in the potential at moderate angular momentum that in turn allows the $\nu g_{9/2}$ structure to appear at fairly low excitation energy and drive deformation.

V. SUMMARY

Yrast and near-yrast states have been studied in ^{55}Cr and ^{55}V using the Gammasphere array at the ATLAS facility. Extended

level schemes for both isotopes have been compared with the results of shell-model calculations using three effective interactions. The GXPF1 family of interactions provides a general agreement with the negative-parity states in ^{55}Cr, while the KB3G interaction has an overall lower rms deviation from the experimental negative-parity level energies in ^{55}V. Negative-parity band structures in ^{55}Cr are revealed as originating from two different configurations: an $f_{5/2}$ neutron outside a ^{54}Cr core and $p_{3/2}$ neutron-hole states relative to $N = 32$. The positive-parity band in ^{55}Cr is reproduced well by projected shell-model calculations and also appears to be characteristic of the smooth band-termination phenomenon. A re-evaluation of the spin-parity assignments in ^{55}V has highlighted the importance of $E3$ transitions deexciting configurations involving $g_{9/2}$ neutrons to the fp shell, and much of the low-lying structure can be reasonably accounted for by shell-model calculations.

[1] A. Huck, G. Klotz, A. Knipper, C. Miehé, C. Richard-Serre, G. Walter, A. Poves, H. L. Ravn, and G. Marguier, Phys. Rev. C **31**, 2226 (1985).
[2] D. E. Appelbe *et al.*, Phys. Rev. C **67**, 034309 (2003).
[3] J. I. Prisciandaro *et al.*, Phys. Lett. B **510**, 17 (2001).
[4] R. V. F. Janssens *et al.*, Phys. Lett. B **546**, 55 (2002).
[5] S. N. Liddick *et al.*, Phys. Rev. Lett. **92**, 072502 (2004).
[6] S. N. Liddick *et al.*, Phys. Rev. C **70**, 064303 (2004).
[7] D.-C. Dinca *et al.*, Phys. Rev. C **71**, 041302(R) (2005).
[8] A. Bürger *et al.*, Phys. Lett. B **622**, 29 (2005).
[9] M. Honma, T. Otsuka, B. A. Brown, and T. Mizusaki, Phys. Rev. C **65**, 061301(R) (2002).
[10] B. Fornal *et al.*, Phys. Rev. C **72**, 044315 (2005).
[11] B. Fornal *et al.*, Phys. Rev. C **70**, 064304 (2004).
[12] M. Honma, T. Otsuka, B. A. Brown, and T. Mizusaki, Eur. Phys. J. A **25**, s01, 499 (2005).
[13] S. Zhu *et al.*, Phys. Lett. B **650**, 135 (2007).
[14] M. Honma, T. Otsuka, and T. Mizusaki, RIKEN Accel. Prog. Rep. **41**, 32 (2008).
[15] F. Perrot *et al.*, Phys. Rev. C **74**, 014313 (2006).
[16] B. Fornal *et al.*, Phys. Rev. C **77**, 014304 (2008).
[17] M. Rejmund, S. Bhattacharyya, A. Navin, W. Mittig, L. Gaudefroy, M. Gelin, G. Mukherjee, F. Rejmund, P. Roussel-Chomaz, and Ch. Theisen, Phys. Rev. C **76**, 021304 (2007).
[18] A. Gade *et al.*, Phys. Rev. C **74**, 021302(R) (2006).
[19] N. Aoi *et al.*, Phys. Rev. Lett. **102**, 012502 (2009).
[20] A. Gade *et al.*, Phys. Rev. C **81**, 051304(R) (2010).
[21] S. Zhu *et al.*, Phys. Rev. C **74**, 064315 (2006).
[22] A. N. Deacon *et al.*, Phys. Lett. B **622**, 151 (2005).
[23] S. J. Freeman *et al.*, Phys. Rev. C **69**, 064301 (2004).
[24] N. Hoteling *et al.*, Phys. Rev. C **77**, 044314 (2008).
[25] W. Rother *et al.*, Phys. Rev. Lett. **106**, 022502 (2011).
[26] S. M. Lenzi, F. Nowacki, A. Poves, and K. Sieja, Phys. Rev. C **82**, 054301 (2010).
[27] K. Hara and Y. Sun, Int. J. Mod. Phys. E **4**, 637 (1995).
[28] Y.-C. Yang, Y. Sun, K. Kaneko, and M. Hasegawa, Phys. Rev. C **82**, 031304 (2010).

[29] Y. Sun, Y.-C. Yang, H.-L. Liu, K. Kaneko, M. Hasegawa, and T. Mizusaki, Phys. Rev. C **80**, 054306 (2009).
[30] S. Zhu *et al.*, Phys. Rev. C **80**, 024318 (2009).
[31] K. Kaneko, Y. Sun, M. Hasegawa, and T. Mizusaki, Phys. Rev. C **78**, 064312 (2008).
[32] A. N. Deacon *et al.*, Phys. Rev. C **76**, 054303 (2007).
[33] I.-Y. Lee, Nucl. Phys. A **520**, c641 (1990).
[34] C. N. Davids, B. B. Back, K. Bindra, D. J. Henderson, W. Kutschera, T. Lauritsen, Y. Nagame, P. Sugathan, A. V. Ramayya, and W. B. Walters, Nucl. Instrum. Methods Phys. Res., Sect. B **70**, 358 (1992).
[35] C. L. Jiang *et al.*, Nucl. Instrum. Methods Phys. Res., Sect. A **554**, 500 (2005).
[36] A. M. Nathan, D. E. Alburger, J. W. Olness, and E. K. Warburton, Phys. Rev. C **16**, 1566 (1977).
[37] D. M. Rosalky, D. J. Baugh, J. Nurzyński, and B. A. Robson, Nucl. Phys. A **142**, 469 (1970).
[38] A. E. MacGregor and G. Brown, Nucl. Phys. A **198**, 237 (1972).
[39] H. Junde, Nucl. Data Sheets **109**, 787 (2008).
[40] P. F. Mantica *et al.*, Phys. Rev. C **68**, 044311 (2003).
[41] P. M. Endt and C. V. D. Leun, At. Data Nucl. Data Tables **13**, 67 (1974).
[42] A. Poves, J. Sánchez-Solano, E. Caurier, and F. Nowacki, Nucl. Phys. A **694**, 157 (2001).
[43] A. Gade *et al.*, Phys. Rev. C **73**, 037309 (2006).
[44] D. Steppenbeck *et al.*, Phys. Rev. C **81**, 014305 (2010).
[45] S. McDaniel *et al.*, Phys. Rev. C **81**, 024301 (2010).
[46] A. N. Deacon *et al.*, Phys. Rev. C **82**, 034305 (2010).
[47] D. Steppenbeck *et al.*, Nucl. Phys. A **847**, 149 (2010).
[48] W. Nazarewicz, J. Dudek, R. Bengtsson, T. Bengtsson, and I. Ragnarsson, Nucl. Phys. A **435**, 397 (1985).
[49] F. R. Xu, P. M. Walker, J. A. Shiekh, and R. Wyss, Phys. Lett. B **435**, 257 (1998).
[50] I. Ragnarsson, V. P. Janzen, D. B. Fossan, N. C. Schmeing, and R. Wadsworth, Phys. Rev. Lett. **74**, 3935 (1995).
[51] A. V. Afanasjev and I. Ragnarsson, Nucl. Phys. A **591**, 387 (1995).
[52] R. Wadsworth *et al.*, Phys. Rev. C **53**, 2763 (1996).